Eur. Phys. J. AP **5**, 283–288 (1999)

THE EUROPEAN PHYSICAL JOURNAL APPLIED PHYSICS

Near-field imaging of the photocurrent on a patterned Au/GaAs interface with various wavelengths and bias*

S. Davy[1], M. Spajer[1,a], J. Almeida[2], R. Generosi[3], A. Cricenti[3], G. Faini[4], and C. Coluzza[5]

[1] Laboratoire d'Optique P.M. Duffieux[b], Institut des Microtechniques[c], UFR Sciences, 25030 Besançon Cedex, France
[2] École Polytechnique Fédérale PH–Ecublens, 1015 Lausanne, Switzerland
[3] CNR-ISM, via E. Fermi 38, 00044 Frascati Roma, Italy
[4] L2M-CNRS, 196 avenue Henri Ravera, B.P. 107, 92225 Bagneux Cedex, France
[5] INFN, Dipartimento di Fisica, Università di Roma "La Sapienza" P. le A. Moro, 00185 Roma, Italy

Received: 02 July 1998 / Revised: 29 September 1998 / Accepted: 13 November 1998

Abstract. This contribution presents an application of scanning near-field optical microscopy to the characterization of semi-conductors. It is based on the photocurrent mapping of a patterned Au/GaAs structure (Schottky barrier) under local illumination by the nanosource. The results obtained with different wavelengths, metallized or dielectric probes and different bias voltages exhibit photocurrent variations independent *of* the topography and induced by interface defects. Finally, from this study of a patterned planar structure, we propose a method to determine the *mean free path* of the charge carriers in the volume.

PACS. 07.79.Fc Near-field scanning optical microscopes – 61.72.Ji Point defects (vacancies, interstitials, color centers, etc.) and defect clusters – 79.60.-i Photoemission and photoelectron spectra

1 Introduction

Scanning Near-Field Optical Microscopy (SNOM) has opened the way to local investigation at a subwavelength scale on devices of optoelectronics or on guiding structures. Dramatic results have been obtained with local spectroscopy of quantum structures [1], field mapping in waveguides [2,3] and in laser cavities [4]. The application to the characterization of semi-conductor multilayer devices transposes to a smaller scale a technique still developed by means of usual optical method (OBIC, optical beam induced current) [5]: the photocurrent induced by the local illumination of a scanning probe is measured during the scanning of the near-field probe. Different configurations have been explored:

- a cross-section of the device can be analyzed, when the probe scans a cleaved face of the multilayer [6–9]. This application requires subwavelength probes to map with a satisfying spatial resolution the photocurrent generated by the different thin layers. The resolution is crucial in the case of the quantum well structures [7];
- the upper surface of the device can be scanned by the tip. In this case the light illuminates the semiconductor through a semi-transparent metallic electrode or through a patterned electrode [6,10–12].

The latter configuration is well-adapted to the detection of inhomogeneities of the various layers of the sample. As in our first experiments achieved with Pt/GaP heterostructure [10], we focus our interest on the carrier transport homogeneity at the Au/GaAs interface.

2 Sample and setup

The sample is made of several layers with different Si doping donors concentrations which are grown on a $n+$ doped GaAs substrate: a 400 nm thick 2×10^{18} cm^{-3} Si-doped buffer is followed by a 170 nm GaAs layer lowering gradually the Si-doping level from 2×10^{18} cm^{-3} to 5×10^{16} cm^{-3}; finally a 1.4 μm thick 5×10^{16} cm^{-3} Si-doped GaAs top layer is grown. A Au–Ge–Ni ohmic contact annealed at 450 °C is deposited in the back side of the structure. Electron beam lithography (EBL) at 50 kV using a JEOL 5DII *e*-beam system is used to define the strips patterns by direct writing on a 150 nm thick PMMA resist spooned on the top side of the wafer. An averaged electron dose of 500 μC cm^{-2} is used for the two lithographic steps at 50 nA and 1 nA spot current required for the patterning. A great care has been taken *of* the preparation of the GaAs surface before the spinning of the PMMA resist using an organic cleaning followed by a 20% HCl aqueous solution to remove the native GaAs

* This paper was presented at the special CFMCP colloquium held at Strasbourg-Illkirch the July 1st-3rd, 1998.

[a] e-mail: michel.spajer@univ-fcomte.fr
[b] UMR 6603 CNRS
[c] FR W0067 CNRS

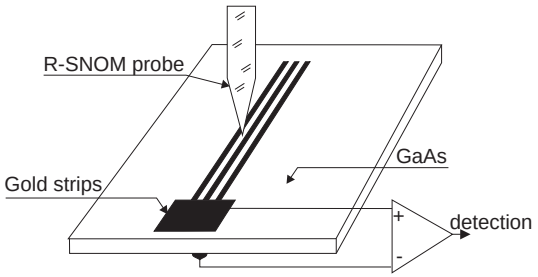

Fig. 1. Sample structure and principle of the experiment.

oxide layer. The Au strips were obtained by the lift-off of 10 nm of Au deposited by electron gun evaporation with a rate of 0.1 nm per second in a 1.5×10^{-7} mbar vacuum chamber. The strips are from 5 μm to 20 μm wide and a few millimeters long. According to literature, the Schottky barrier of this structure is $V_{\mathrm{FB}} = 0.9$ eV [13]. This value involves *that some* specific laser source *allows* to distinguish the current due to internal photoemission at the interface from the photoconductivity of the semiconductor: the energy of the photons must be higher than the Schottky barrier ($\lambda < 1.39$ μm), but lower than the conduction gap.

The principle of the experiment is based upon a reflection SNOM (R-SNOM) [14] and is schematized by Figure 1: the sample is scanned by a nanosource made of a tapered fiber obtained under a CO_2 laser beam with a commercial micro-pipette puller. Such a probe has typically a 80 nm tip diameter and can be coated in a vacuum chamber by a 100 nm thick aluminum layer except the extremity. The tip is maintained a few nanometers from the sample surface by a shear-force mechanism and the photocurrent is recorded simultaneously with the topography of the gold structure. The lasers we used supply a power of a few mW (from 3 to 10 mW) at five different wavelengths: $\lambda = 543$ nm, 632 nm, 782 nm, 850 nm and 1.33 μm. We observed also the modifications of the photocurrent mapping by a bias voltage on the junction. All the images presented in the next section have a dimension of 30 μm $\times$ 30 μm. In each of them, the aberrant first lines (top of the image) are due to the opened shear force feedback loop at the beginning of the scanning. Ignoring this exception, the shear-force image has a resolution better than 1 nm in z direction.

3 Results with metallized tips

Figure 2 shows a set of images obtained with a metallized tip connected to a 6 mW laser diode emitting at $\lambda =$ 782 nm.

The maximum intensity of the photocurrent is of the order of 10 pA and is quite correlated to the position of the gold strips, which is given by the shear-force image. The sharpness of the edges is here a qualitative indication of the good resolution capability of the apertured probe, but a more precise evaluation is difficult, due to several electronic phenomena, as it will be seen on the next images.

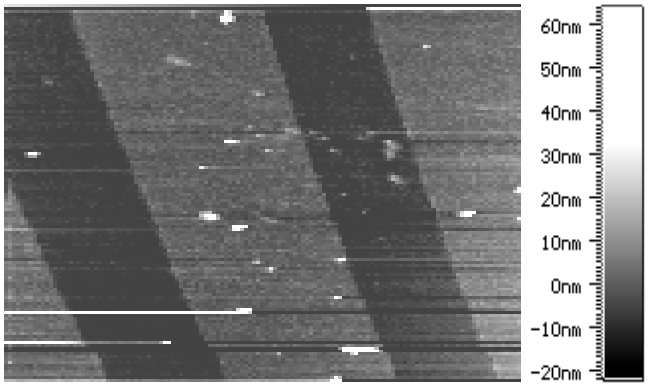

(a)

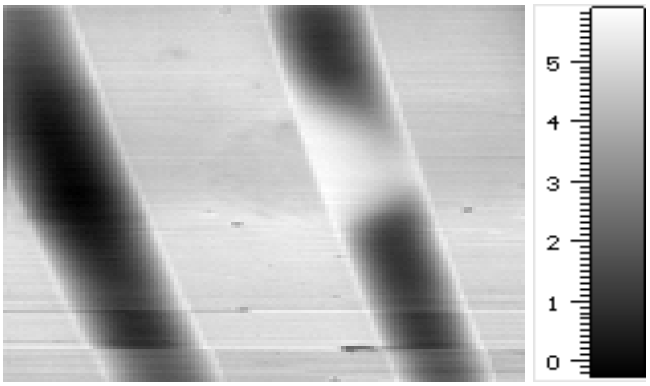

(b)

Fig. 2. Images with metallized tip and $\lambda = 782$ nm. (a) Topographic image 30 $\times$ 30 μm, (b) photocurrent image.

Besides, the interruption of the trough in the middle of Figure 2b joined by a quasi inverted contrast is correlated to a slight topographical defect and remains unexplained: they can be due to a defect in the fabrication of the layers, in the masking process or in the metal deposition.

A second set of experiments have been carried out with a *new metallized tip* in the near infra-red domain (including at 782 nm, as the probe was different than in the previous experiment) with different laser diodes and a titanium-sapphire tunable laser. We have observed that the gold strips are not resolved in the same way by the different wavelengths. Figure 3a shows the cross-section of the photocurrent for 4 wavelengths. Each curves is characterized by 2 parameters: the Full Width Half Maximum (FWHM) of the unmetallized area and the slope over the gold edge. The trend of their variations is schematized by Figure 3.

In order to discuss the evolution of these curves, we must take *into* account different parameters:

- the photon energy: *for an* energy higher than 1.42 eV ($\lambda < 880$ nm), some carriers are also created in the GaAs bulk, between the gold strips;
- the *density* of the localized surface states on GaAs surface and the interface states which can trap the charge carriers;

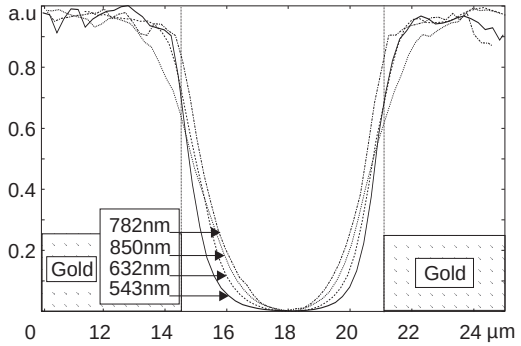

(a)

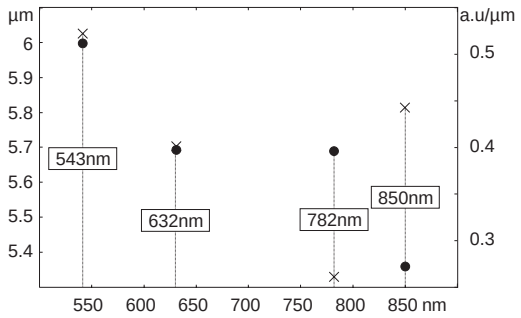

(b)

Fig. 3. Resolution of the photocurrent with respect to the wavelength. (a) Cross-section of the photocurrent over the gold strips, (b) slope (•, right scale) and FWHM (×, left scale) of the photocurrent over the non-metallized area *vs.* wavelength.

Table 1. Complex *refractive* index of GaAs for different wavelengths and penetration coefficient of the photon inside the GaAs bulk.

λ (μm)	n	k	$1/\alpha$ (μm)
0.543	4.082	0.308	0.14
0.632	3.856	0.196	0.256
0.782	3.693	0.089	0.7
0.850	3.666	0.0612	1.1
1.33	3.409	0	∞

– the penetration *depth* of the photons which increases with the wavelength.

Table 1 shows [15] the complex refractive index $n_c = n - ik$ of gallium arsenide. The k coefficient is related to the absorption of the photon into the material: if I_i is the incident intensity at the surface, the intensity $I(z)$ at a distance z from the surface is given by:

$$I(z) = I_i e^{-\alpha z} \quad \text{with} \quad \alpha = \frac{4\pi}{\lambda} k.$$

The thickness W of the depletion region is given by

$$W = \sqrt{\frac{2\epsilon_s(\Phi_i - kT)}{q^2 N_d}}$$

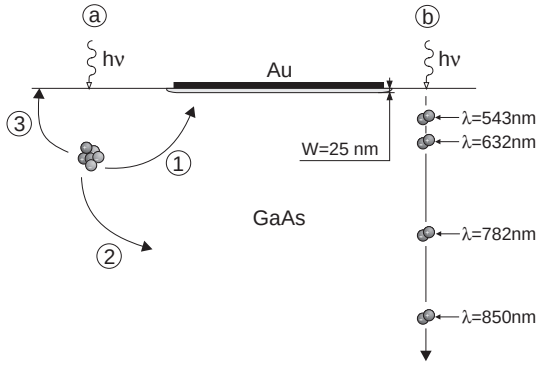

Fig. 4. (a) Recombination mechanisms of the charge carriers. 1: photocurrent contribution, 2: recombination in the volume, 3: recombination at the surface. (b) comparison between W and $1/\alpha$ for different wavelengths.

where ϵ_s is the permitivity of the semi-conductor and

$$q\Phi_i = qV_{FB} - kT \ln \frac{N_c}{N_d}$$

is the distance between the conduction band and the Fermi level (N_c is the effective density of states in conduction band (4.7×10^{17} cm^{-3} for GaAs), N_d the donors concentration, Φ_i the built-in-potential, k the Boltzman constant, T the temperature). This gives a value of $W = 25$ nm. Figure 4 shows the comparison between W and the penetration of the light at a distance $1/e$ inside the semiconductor.

When an electron/hole pair is generated by fundamental absorption of a photon between the strips, the minority carriers have several possibilities (Fig. 4):

1. they can contribute to the photocurrent if they are close enough (inside the diffusion length) to the junction;
2. they can be trapped inside the bulk (hole/electron recombination, which is mainly non radiative in GaAs);
3. they can recombine at the surface due to the presence of localized surface states, without contributing to the photocurrent.

Surface recombination is due to the break-up of the lattice at the buffer/air interface and to the presence of impurities. For GaAs, the surface states density is around 12.5×10^{13} eV cm^{-2} (10 times greater than for Si). For the shorter wavelengths, the carrier is generated close enough to the surface to be trapped. This can explain the highest FWHM value is obtained for $\lambda = 543$ nm. As the wavelength increases, the free carriers are generated more deeply into GaAs, surface recombination plays a minor role, and carriers collected by the strips can contribute to the photocurrent, which decreases the FWHM. Besides, as the wavelength increases, the carriers can be generated far away from the depletion region and they can recombine into the bulk. The trend in these conditions is to increase again the FWHM.

Therefore, bulk recombination is probably responsible of the non-monotonous behaviour of the FWHM under

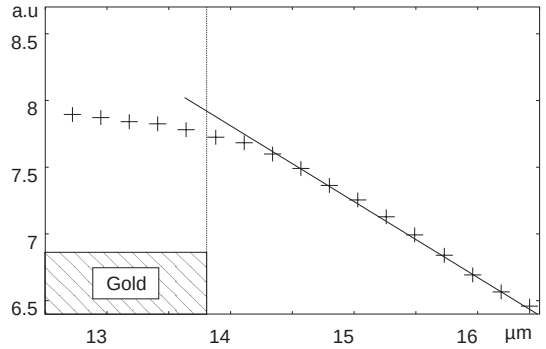

Fig. 5. Logarithm of the photocurrent with respect to the lateral distance for $\lambda = 850$ nm. The slope gives $L = 1.76$ μm for the diffusion length.

the condition that the aperture has a sufficient dimension to emit enough propagating light inside the substrate. This would be in agreement with the evaluation of Ünlü *et al.* [8]: the resolution depends on the wavelength if the tip aperture is larger than $\lambda/2n$, *i.e.* the value of half-the-wavelength inside the semi-conductor. This condition, applied to GaAs at $\lambda = 850$ nm, the *refractive* index of which is $n = 3.666$, involves that our tip diameter is larger than 115 nm.

As a first conclusion, the shorter wavelengths are more efficient for edge resolution and the photocurrent images measured with the longer wavelengths seem more sensitive to the bulk characteristics. Therefore, it is possible to determine the diffusion length of the minority carriers in the bulk GaAs. Moving a few nanometers *beside* the gold edge, the photocurrent level depends only on the dominant recombination mechanism. Its variations *versus* the distance x from the gold edge is related to the diffusion of the carriers in the volume and can be considered as an exponential decrease [7]

$$I = I_0 \mathrm{e}^{-x/L}$$

where L is the diffusion length of the minority carriers and I_0 the photocurrent measured at the gold strip edge. Figure 5 shows the logarithm of the photocurrent *versus* the distance to the gold strip edge for $\lambda = 850$ nm. The curve exhibits a good linear behavior (correlation coefficient = 0.9988) and the slope gives the diffusion length of the minority carriers: $L = 1.76$ μm. This kind of measurements is usually done on a plane perpendicular to the junction (cleaved sample), for example with SNOM or STM probe. Here the computation is carried out from a planar structure because the wavelength which is used generates the carriers deep into the bulk. Using a shorter wavelength, for example in the blue or in UV, we could obtain information about the surface recombination velocity and the presence of a dead layer.

4 Results using dielectric tips

Our attempts to measure the photocurrent induced at 1.33 μm with metallized tips failed, mainly because the photon energy is smaller than the GaAs photoconductivity threshold ($\lambda = 880$ nm), so the only phenomenon responsible of the carriers generation is internal photoemission. This low efficiency and the low throughput of the metallized tip led us to use dielectric probes. Nevertheless the resolution is the best we obtained for two reasons:

- the GaAs is quasi-transparent at this wavelength and there is no emission out of the gold strip;
- the field confinement around the tip is sufficient to reach a subwavelength resolution, as shown for example in reference [16] for a photolithographic experiment.

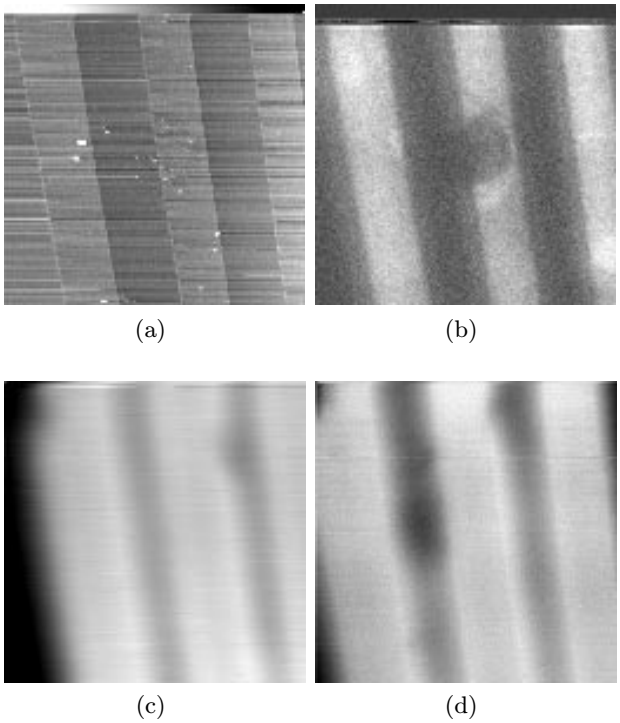

Fig. 6. Images with a dielectric tip and different wavelengths on the same area. The photocurrent image (b) is not "polluted" by photoconduction. (a) Topography 30×30 μm, (b) $\lambda = 1.33$ μm, (c) $\lambda = 782$ nm, (d) $\lambda = 632$ nm.

Figure 6b gives the best image of photocurrent lateral variations uncorrelated with the topography or with gold damaging. The same *flaw* is no more visible in Figures 6c and 6d, despite the higher photocurrent level obtained at 632 nm and 782 nm (around 1 nA instead of 10 pA). It means that measurements done at a wavelength close to the threshold characterize the metal/semi-conductor interface. It must also be observed that the scratches are less contrasted on the photocurrent images of this figure than in Figure 2b, as expected in a transmission near-field image obtained with a dielectric probe.

In order to improve the resolution with dielectric tips, we have biased (*cf.* Fig. 1) the junction: the applied voltage changes the band bending at the junction. This modification induces some variations on the carrier collection.

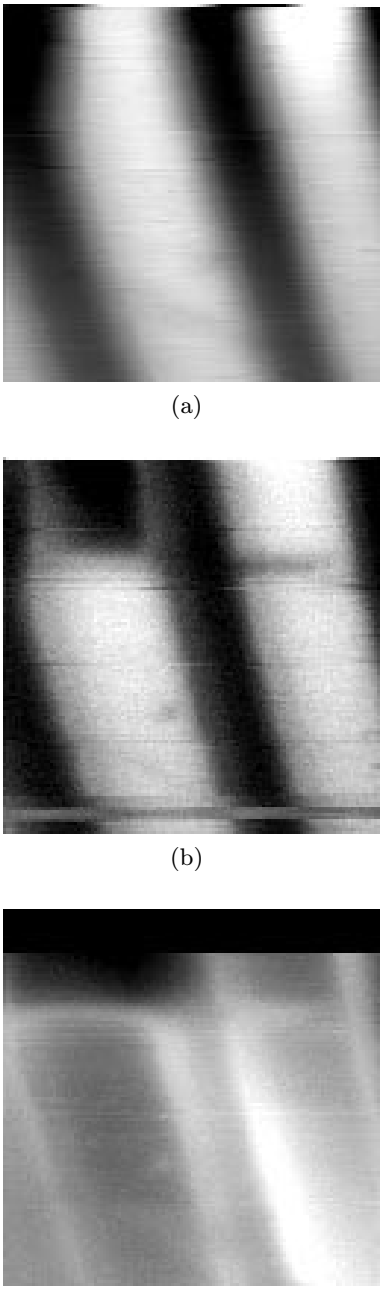

(a)

(b)

(c)

Fig. 7. Photocurrent images 30×30 μm at 543 nm with different bias. Notice the 2 details at the bottom of the image and the variations of their resolution and contrast with the bias. (a) $U = 0$ V, (b) $U = -1.5$ V, (c) $U = +0.3$ V.

Figure 7 shows 3 images at $\lambda = 543$ nm with different applied bias.

Applying a reverse voltage (-1.5 V, Fig. 7b) improves the photocurrent lateral resolution, as it can be seen from the edge sharpness and from some details in the lower part of the image (a dot and a segment which are perhaps due to the presence of thin oxide layer at the interface). The negative bias increases the junction electrical field and therefore the collection efficiency. The dark photocurrent area visible on the higher part of the left strip suggests that the electric field is weaker than on bright areas. Several phenomena can be responsible of these inhomogeneities:

- the high *resistance* of the metal due to the low thickness of the metal layer;
- the metal thickness variations;
- the presence of scratches.

A forward bias voltage (+0.3 V, Fig. 7c) decreases the band bending and the collection efficiency , until zero photocurrent in flat-band condition and increases the recombination mechanisms in the depletion region. This voltage condition exhibits a very different photocurrent pattern, with an enhancement of strip edge. The range of photocurrent on this image is around 3 times smaller than on image 7b and the photocurrent level on the GaAs is roughly the same than on gold strip. Thus the edge effects are more enhanced than on image 7b. These edge effects are due to the curvature of the depletion region at the gold edge which increases the electric field intensity. This phenomenon is well-known in Schottky structure technology: it is possible to "smooth" the curvature of the depletion region, for example making a *guard ring* by the implantation of a $p+$ doped region at the gold edge. Here, no special care has been taken to attenuate the edge effects.

In the non metal areas situated very close to the metal contact (*e.g.* in the GaAs near the gold and in the scratches) the electric field is not reduced by the forward bias and penetrates deeper into the GaAs. This can explain why the edge effects are so enhanced on this image. In general, the applied bias reveals significant defects on the studied patterned Schottky barrier, showing the capabilities of SNOM in microanalysis.

Another reason for using dielectric tip comes from a *thermal* point of view. Some studies on the temperature distribution in metallized tips show that this temperature can reach 300 °C [17,18]. Given the weak thickness of the strips, their resistivity could be locally influenced by the heating of the tip which could influence the results. This effect would be less important with a dielectric tip which is "colder".

5 Conclusion

The comparison of the photocurrent images obtained at different wavelengths confirms the possibility of detecting subwavelength interface *defects* when the excitation wavelength is close to the threshold of the Schottky barrier. Since the semi-conductor is optically transparent for such a wavelength, the internal photo-emission is *dominating* on bulk effects. To compensate the very low photocurrent intensity, only bare tapered tips have been used. However, despite the risk of stray light due to such uncoated fiber, the experimental results demonstrate clearly subwavelength resolution properties for certain wavelengths.

Let us notice that the spatial resolution at short wavelengths can be improved by addition of a reverse bias

voltage. To determine the diffusion length of the minority carriers in the volume, a method using a planar structure has been implemented. To complete this measurement, the differences in carrier distribution with respect to the wavelength could be studied.

Finally, it must be emphasized that the scanning near field optical microscope can be a real competitor to the confocal microscope because it provides in a simple way both an optical image (or here a photocurrent mapping) with submicrometer resolution and an absolute topographical image.

This work is supported by a grant from Jobin-Yvon ISA and CNRS (No. 062004000).

References

1. A. Richter, M. Sueptitz, C. Lienau, T. Elsaesser, R. Nötzel, M. Ramsteiner, K. Ploog, Quantum wire, in *4th International Conference on Near-Field Optics*, Jerusalem, 1997, p. 17.
2. R. Cella, B. Mersali, A. Bruno, S. Davy, H.J. Brückner, C. Licoppe, J. Appl. Phys. **78**, 4339 (1995).
3. N.V. Hulst, M. Moers, E. Borgonjen, Application of near-field optical microscopy: fluorescence *in situ* hybridisation, Langmuir-Blodgett films and integrated optical waveguides, in *Photons and Local Probes*, edited by O. Marti, R. Möller (Kluwer Academic Publishers, 1995), pp. 165–180.
4. I. Hörsch, R. Kushe, O. Marti, B. Weigl, K.J. Ebeling, J. Appl. Phys. **79**, 3831 (1996).
5. T. Wilson, C. Sheppard, *Theory and practice of scanning optical microscopy* (Academic Press, London, 1984).
6. K. Karrai, G. Kolb, G. Abstreiter, A. Schmeller, Ultramicroscopy **61**, 299 (1995).
7. S.K. Buratto, J.W.P. Hsu, E. Betzig, J.K. Trautman, R.B. Bylsma, C.C. Bahr, M.J. Cardillo, Appl. Phys. Lett. **65**, 2654 (1994).
8. M.S. Ünlü, B.B. Goldberg, W.D. Herzog, Appl. Phys. Lett. **67**, 1862 (1995).
9. B.B. Goldberg, M.S. Ünlü, W.D. Herzog, H.F. Ghaemi, E. Towe, IEEE J. Quant. Electr. **1**, 1073 (1995).
10. J. Almeida, T. dell'Orto, C. Coluzza, G. Margaritondo, O. Bergossi, M. Spajer, D. Courjon, Appl. Phys. Lett. **69**, 2361 (1996).
11. J.W.P. Hsu, E.A. Fitzgerald, Y.H. Xie, P.J. Silverman, Appl. Phys. Lett. **65**, 344 (1994).
12. J.W.P. Hsu, E.A. Fitzgerald, Y.H. Xie, P.J. Silverman, J. Appl. Phys. **79**, 7743 (1996).
13. E.H. Rhoderick, R.H. Williams, *Metal-semiconductor contacts* (Clarendon, Oxford, 1988).
14. D. Courjon, J.M. Vigoureux, M. Spajer, K. Sarayeddine, S. Leblanc, Appl. Opt. **29**, 3734 (1990).
15. E.D. Palik, *Handbook of optical constants of solids* (Academis Press, 1985).
16. S. Davy, M. Spajer, Appl. Phys. Lett. **69**, 3306 (1996).
17. M. Stähelin, M.A. Bopp, G. Tarrach, A.J. Meixner, I. Zschokkle-Gränacher, Appl. Phys. Lett. **68**, 2603 (1996).
18. B.I. Yakobson, A. LaRosa, H.D. Hallen, M.A. Paesler, Ultramicroscopy **61**, 179 (1995).